J Neurophysiol 103: 1798–1808, 2010.
First published January 27, 2010; doi:10.1152/jn.91235.2008.

The Effect of Noise on CaMKII Activation in a Dendritic Spine During LTP Induction

Shangyou Zeng[1] and William R. Holmes[2]

[1]*College of Electronic Engineering, Guangxi Normal University, Guangxi, China; and* [2]*Neuroscience Program, Department of Biological Sciences, Ohio University, Athens, Ohio*

Submitted 12 November 2008; accepted in final form 22 January 2010

Zeng S, Holmes WR. The effect of noise on CaMKII activation in a dendritic spine during LTP induction. *J Neurophysiol* 103: 1798–1808, 2010. First published January 27, 2010; doi:10.1152/jn.91235.2008. Activation of calcium-calmodulin dependent protein kinase II (CaMKII) during induction of long-term potentiation (LTP) is a series of complicated stochastic processes that are affected by noise. There are two main sources of noise affecting CaMKII activation within a dendritic spine. One is the noise associated with stochastic opening of *N*-methyl-D-aspartate (NMDA) receptor channels and the other is the noise associated with the stochastic reaction-diffusion kinetics leading to CaMKII activation. Many models have been developed to simulate CaMKII activation, but there is no fully stochastic model that studies the effect of noise on CaMKII activation. Here we construct a fully stochastic model to study these effects. Our results show that noise has important effects on CaMKII activation variability, with the effect from stochastic opening of NMDA receptor channels being 5–10 times more significant than that from stochastic reactions involving CaMKII. In addition, CaMKII activation levels and the variability of activation are greatly affected by small changes in NMDA receptor channel number at the synapse. One reason LTP induction protocols may require tetanic or repeated burst stimulation is that there is a need to overcome inherent variability to provide sufficiently large calcium signals through NMDA receptor channels; with meaningful physiological stimuli, noise may allow the calcium signal to exceed threshold for CaMKII activation when it might not do so otherwise.

INTRODUCTION

One of the most studied phenomena in neuroscience over the past three decades is long-term potentiation (LTP). LTP is a modification of synaptic strength originally discovered in the dentate and is the best model we have of how memory and learning occur (Bliss and Collingridge 1993; Malenka and Nicoll 1993). In the most studied form of LTP, high levels of calcium influx through *N*-methyl-D-aspartate (NMDA) receptor channels at synapses on dendritic spines activate calcium/calmodulin-dependent protein kinase II (CaMKII) to induce LTP (Lisman 2003; Lisman et al. 1997; Malenka and Bear 2004). The calcium that enters the spine head from the synaptic cleft binds to calmodulin to produce the calcium–calmodulin complex that can bind to individual subunits of CaMKII and activate them. When enough CaMKII subunits are activated, autophosphorylation can occur (Miller and Kennedy 1986), which traps calmodulin on a subunit and makes the subunit active long after the calcium signal is over (Meyer et al. 1992). The actions of activated CaMKII induce LTP (Fukunaga et al. 1993, 1996; Lisman et al. 2002).

Address for reprint requests and other correspondence: W. R. Holmes, Neuroscience Program, Dept. of Biological Sciences, Ohio Univ., Athens, OH 45701 (E-mail: holmes@ohio.edu).

There are many types of noise in the nervous system (Ermentrout et al. 2008; Faisal et al. 2008). Three main types of noise in neurons are thermal noise (Jaramillo and Wiesenfeld 1998; Johnson 1987; Shimozawa et al. 2003), ion channel noise (Clay and DeFelice 1983; White et al. 2000), and synaptic noise (Calvin and Stevens 1967; Fellous et al. 2003). Noise in neural systems has important effects on many neural processes, such as spike generation (Faisal and Laughlin 2007; Zeng and Jung 2004), information transmission (Bezrukov and Vodyanoy 1995; Hoch et al. 2003; Yu et al. 2001; Zeng et al. 2007), perception (Shimozawa et al. 2003), and the observed trial-to-trial variability in LTP (Malenka and Nicoll 1993; Malinow and Tsien 1990). In particular, CaMKII activation, which leads to LTP induction, is a series of stochastic reaction-diffusion processes that are subject to noise. Others have shown that noise can affect the induction and stability of the CaMKII switch (Bhalla 2004a,b; Graupner et al. 2007; Hayer and Bhalla 2005; Miller and Wang 2006; Miller et al. 2005), which is implicated in LTP/long-term depression (LTD) and long-term memory (Lisman and Zhabotinsky 2001; Lisman et al. 2002). Thus it is important to understand the effect of noise on CaMKII activation.

There are many sources of noise that affect CaMKII activation within a dendritic spine. One source is the stochastic opening of NMDA receptor channels (Chen et al. 1999; Rosenmund et al. 1995). Another is the stochastic reaction-diffusion kinetics leading to CaMKII activation within a dendritic spine, which includes stochastic binding of calcium to calmodulin (Keller et al. 2008), stochastic binding of calmodulin to CaMKII (Byrne et al. 2009), stochastic calmodulin trapping, and stochastic calcium-independent autophosphorylation (Franks and Sejnowski 2004; Xia and Storm 2005). Models have been developed to simulate how the calcium signal leads to calmodulin trapping and CaMKII activation (Coomber 1998; Dosemeci and Albers 1996; Holmes 2000; Kubota and Bower 2001; Matsushita et al. 1995; Michelson and Schulman 1994; Okamoto and Ichikawa 2000; Zhabotinsky 2000; Zhabotinsky et al. 2006). In most of these models, the calcium signal was considered to be an arbitrary wave form, and binding of calcium to calmodulin, calmodulin trapping, and calcium-independent autophosphorylation were treated deterministically. However, because of the small numbers of some components in these reactions, these processes should be treated stochastically.

Here we use a stochastic model of reaction and diffusion at a synapse to determine NMDA receptor channel openings. These NMDA receptor channel openings are used in a neuron level model to compute calcium influx through NMDA receptor channels in dendritic spines following tetanic input to

hundreds of synapses in a model of a fully reconstructed dentate granule cell. This calcium influx is used in a fully stochastic model of calcium dynamics in a dendritic spine to simulate binding of calcium to calmodulin, calmodulin trapping, and calcium-independent autophosphorylation. We find that CaMKII activation can be highly sensitive to stochastic openings of NMDA receptor channels. The effect from stochastic openings of NMDA receptor channels is almost 5–10 times larger than that from noise in the stochastic reactions leading to CaMKII activation. In addition, CaMKII activation is greatly affected by small changes in the number of NMDA receptors at a synapse.

METHODS

Generation of the calcium input signal

The calcium input signal is calculated with the use of synapse and neuron level models as described in Holmes (2000), except that here the opening of NMDA receptor channels is modeled stochastically at the synapse of interest. In the synapse level model, glutamate (2,000 molecules) is released into the synaptic cleft where it diffuses, gets pumped into neurons or glia by glutamate transporters, or binds to NMDA and AMPA receptors, leading to the opening of NMDA and AMPA receptor channels at the synapse. This process is computed deterministically at most synapses (Holmes 1995) but stochastically with MCell v. 2.50 (Stiles and Bartol 2001) at the synapse of interest. For a fixed number of AMPA and NMDA receptors, the locations of receptors and glutamate uptake transporters was identical across trials to eliminate variability of receptor location as a source of noise. The time course of the number of open NMDA and AMPA receptor channels is used at synapses in a neuron level model of a fully reconstructed dentate granule cell with voltage-dependent conductances on the soma, axon, and proximal dendrites (Holmes and Levy 1997). Activation of 300 excitatory synapses on the dendritic spines in the middle third of the dendritic tree is modeled to represent strong medial perforant path (mpp) input. These synapses are activated with a single stimulus train of eight presynaptic spikes at frequencies of 10–400 Hz. The voltage computed in the neuron level model is used to determine the number of open NMDA channels (from the synapse level model) that are not blocked by magnesium. Blockage by magnesium is modeled deterministically except at the synapse of interest where it is modeled stochastically. Given a single channel conductance of 50 pS for NMDA receptor channels, the number of open, unblocked channels at the synapse, and the voltage at the synapse, the NMDA current at the synapse can be computed. The calcium portion of the NMDA current is computed with the constant field equation. This calcium portion of the NMDA current is used as the calcium signal in the spine model described below.

MCELL MODEL DETAILS. The parameters of the synapse model including the reaction schemes for NMDA and AMPA receptor channels were those used previously (see Holmes and Levy 1997 for reaction schemes and Holmes 1995 for cleft parameters). In MCell, the synaptic cleft was a box $8 \times 8 \times 0.02$ μm with the vesicle release site located at the center of the top of the box and the postsynaptic density (PSD) located at the center of the bottom of the box. A synaptic vesicle 0.05 μm in diameter released 2,000 glutamate molecules into the synaptic cleft. The glutamate diffusion constant was 0.25×10^{-5} cm^2/s. The PSD radius was 0.1 μm. We chose NMDA and AMPA receptor densities to match different numbers of NMDA and 63 AMPA receptors. However, MCell 2 randomly assigns receptor number from the density values (and also location), and this means different seeds will produce different numbers of receptors for the same densities. We ran simulations with different seeds to find a set of seeds that would give us, for example, 14 and 63 NMDA and non-NMDA receptors, respectively. A seed that gave us the desired number of receptors was selected and was used for one time step to fix the locations of NMDA receptors, AMPA receptors, and glutamate uptake transporters. Making use of MCell's checkpoint feature, we chose a different seed for each of 30 simulation trials to simulate all subsequent time steps. We note that this did not fix the number of glutamate uptake transporters across simulations with different numbers of NMDA receptors because MCell assigns transporter number and location randomly. It was not possible to find seeds that gave the same exact uptake environment for every desired combination of NMDA and AMPA receptors. To make uptake characteristics as consistent as possible across all simulations, we modified uptake rate constant values. Specifically, we model neuronal and glial glutamate uptake with Michaelis-Menten kinetics with fixed K_m and V_{max} values for each type of uptake as in Holmes (1995); this does not fix transporter density and transporter uptake rate independently, so in MCell, we fixed uptake transporter density and modified the two forward rate constants in the Michaelis-Menten scheme to match V_{max} and K_m based on the number of transporter molecules MCell decided to choose for density for a particular random seed from the density value (backward rate constants were assumed to be zero).

COMPUTING THE CALCIUM COMPONENT OF THE NMDA CURRENT. The number of open NMDA receptor channels as a function of time computed with MCell was read into the neuron level model for the synapse of interest. When a channel became open, it was assigned randomly to be either open or blocked according to the probabilities computed from kinetic rates reported by Ascher and Nowak (1988). At each time step, each open NMDA channel and each blocked NMDA channel was interrogated to determine whether the channel would change state, given the voltage at the synapse and the probabilities of switching states. If the MCell input indicated that a channel closes, probabilities based on the rate constants were again used to decide if a blocked channel closed or an open channel closed. Extracellular magnesium concentration was 1.2 mM. The dentate granule cell model computes $I_{NMDA} = g_{NMDA}(V - V_{NMDA})$, where g_{NMDA} is the number of open, unblocked NMDA receptor channels multiplied by 50 pS, the single channel conductance. Given the ion concentrations, V_{NMDA} was +1.3827 mV, slightly larger than the value of 0 mV usually used. To separate out the calcium component, we use the procedure from Holmes and Levy (1990), which is based on the analysis by Mayer and Westbrook (1987) using the Goldman-Hodgkin-Katz (GHK) constant field current equations and ion activities. From *Eqs. 3* and *4* from Mayer and Westbrook (1987), we get

$$I_{NMDA} = I_{Na} + I_K + I_{Ca} = P_{Na}c + P_K d + P_{Ca}e$$

where

$$I_{Na} = P_{Na}c = P_{Na}\frac{VF^2}{RT}\frac{[Na^+]_i - [Na^+]_o \exp(-VF/RT)}{1-\exp(-VF/RT)}$$

$$I_K = P_K d = P_K\frac{VF^2}{RT}\frac{[K^+]_i - [K^+]_o \exp(-VF/RT)}{1-\exp(-VF/RT)}$$

$$I_{Ca} = P_{Ca}e = P_{Ca}\frac{4VF^2}{RT}\frac{[Ca^{++}]_i - [Ca^{++}]_o \exp(-2VF/RT)}{1-\exp(-2VF/RT)} \quad (1)$$

Mayer and Westbrook (1987) report that P_{Na}:P_K:P_{Ca} = 1:1:10.6. Substituting in the preceding equations, we get $I_{NMDA} = P_{Na}(c + d + 10.6e)$. This is solved for P_{Na}, and $I_{Ca} = 10.6P_{Na}e$. Mayer and Westbrook (1987) found better fits to the data when they used ion activities instead of concentrations. Thus the concentrations given in the preceding equations were multiplied by their activity coefficients in our computations. We use 10 mM Na^+, 140 mM K^+, and 20 nM Ca^{2+} inside the cell and 145 mM Na^+, 2.5 mM K^+, and 2 mM Ca^{2+} outside. Activity coefficients are 0.75 for Na^+, 0.75 for K^+, and 0.19 for Ca^{2+}, and temperature is 37°C making RT/F 26.73.

Stochastic simulation of reaction and diffusion

Stochastic reactions in a homogeneous volume are often modeled with the Gillespie algorithm (Gillespie 1976, 1977). However, the living cell is usually a spatially complicated system that is not homogeneous. Therefore the Gillespie method has to be adjusted to fit the heterogeneous system. A typical solution for spatially heterogeneous coupled reaction-diffusion systems is to divide the system into many voxels, which can be considered as homogeneous (Gillespie 1976). The homogeneous Gillespie's method can be applied to each individual voxel. We will briefly describe the Gillespie algorithm in one volume and show how we extend it to heterogeneous volumes.

First consider reactions within one homogeneous volume. A system consisting of coupled chemical reactions may contain reactions ($R_1, \ldots, R_K$), each having the following stoichiometric form

$$R_{\mu\,(\mu=1\ldots K)}\colon m_1^\mu S_1 + m_2^\mu S_2 + \ldots + m_N^\mu S_N \xrightarrow{c_\mu} n_1^\mu S_1 + n_2^\mu S_2 + \ldots + n_N^\mu S_N \quad (2)$$

where c_μ is the stochastic reaction rate parameter for reaction μ and the m_1^μ and n_1^μ are the stoichiometric coefficients of species S_i in reaction μ. The stochastic reaction rate parameter c_μ has a simple relationship to the traditional deterministic rate constant k_μ, which mathematically depends on the stoichiometric coefficients and the volume in which the reactions take place (Gillespie 1976).

If there are $X_1, \ldots, X_N$ molecules of species $S_1, \ldots, S_N$, the number of distinct reactant combinations, h_μ, for reaction μ is

$$h_\mu = \prod_{a=1}^{N} \binom{X_a}{m_a} \quad (3)$$

Given the number of distinct reactant combinations and the stochastic rate parameter c_μ, the probability of reaction μ occurring in unit time is $a_\mu = h_\mu c_\mu$. The sum of the probabilities over all reactions is

$$a = \sum_{\mu=1}^{K} a_\mu = \sum_{\mu=1}^{K} h_\mu c_\mu \quad (4)$$

According to the Gillespie algorithm, one can determine the time of the next reaction and the identity of the next reaction by drawing two uniformly distributed random numbers r_1 and r_2. The time of the next reaction τ is

$$\tau = -\ln(r_1)/a \quad (5)$$

and the identity of the next reaction is reaction μ satisfying

$$\sum_{j=1}^{\mu-1} a_j < a r_2 < \sum_{j=1}^{\mu} a_j \quad (6)$$

The simulation is advanced a time step τ and the numbers of molecules $X_1, \ldots, X_N$ of species $S_1, \ldots, S_N$ are updated according to the stoichiometry of reaction μ.

Although this algorithm is straightforward to implement, it is valid only for a homogeneous well-mixed volume. To use this algorithm for an inhomogeneous volume, the volume is divided up into voxels that individually are homogeneous and well mixed. Gillespie suggested a method based on Fick's first law of diffusion $j = -D\nabla C$, where flux j can be interpreted as the number of diffusing ligands that cross the unit surface in unit time. The diffusion of a molecule of species α from voxel V_l into its neighbor V_{l+1} can be simulated as a special reaction consisting of two simultaneous subreactions: $S_\alpha \rightarrow *$ (destroyed) in V_l and $* \rightarrow S_\alpha$ (created) in V_{l+1}. By Fick's first law of diffusion, the probability coefficient d_α can be obtained as

$$d_\alpha = D_\alpha A_{l,l+1}[(X_{l,\alpha}/V_l) - (X_{l+1,\alpha}/V_{l+1})]/b_{l,\,l+1}, \quad \text{if } X_{l,\alpha}/V_l > X_{l+1,\alpha}/V_{l+1}$$
$$= 0 \quad \text{otherwise} \quad (7)$$

where, $b_{l,l+1}$ is the center-to-center distance between the two adjacent subvolumes, $A_{l,l+1}$ is the interfacing area between the two adjacent subvolumes, D_α is the diffusion constant for species α, and $X_{l,\alpha}$, $X_{l+1,\alpha}$ are the numbers of molecules of the species α in the adjacent subvolumes V_l and V_{l+1}, respectively.

The a defined by *Eq. 4* is modified to include the probabilities for all reactions and all diffusions in all voxels

$$a = \sum_{i=1}^{N_x}\sum_{j=1}^{N_y}\sum_{k=1}^{N_z}\left(\sum_{\mu=1}^{K} h_{\mu,ijk}c_\mu + \sum_{\alpha=1}^{N} X_{\alpha,ijk}d_\alpha\right) \quad (8)$$

where N_x, N_y, and N_z are the numbers of voxels in the x, y, and z dimensions, respectively. As before, the time of the next reaction and the identity of the next reaction (or diffusion) are determined by drawing two random numbers r_1 and r_2. The time of the next reaction is still computed with *Eq. 5*, but a is now defined by *Eq. 8*. The identity of the next reaction or diffusion is determined from the following extensions of *Eq. 6*

$$\sum_{i=1}^{i'-1}\sum_{j=1}^{j'-1}\sum_{k=1}^{k'-1}\left(\sum_{\mu=1}^{\mu'-1} h_{\mu,ijk}c_\mu\right) < r_2 a \le \sum_{i=1}^{i'}\sum_{j=1}^{j'}\sum_{k=1}^{k'}\left(\sum_{\mu=1}^{\mu'} h_{\mu,ijk}c_\mu\right) \text{(reaction)} \quad (9a)$$

or

$$\sum_{i=1}^{i'-1}\sum_{j=1}^{j'-1}\sum_{k=1}^{k'-1}\left(\sum_{\mu=1}^{K} h_{\mu,ijk}c_\mu + \sum_{\alpha=1}^{\alpha'-1} X_{\alpha,ijk}d_\alpha\right) < r_2 a \le \sum_{i=1}^{i'}\sum_{j=1}^{j'}\sum_{k=1}^{k'}\left(\sum_{\mu=1}^{K} h_{\mu,ijk}c_\mu + \sum_{\alpha=1}^{\alpha'} X_{\alpha,ijk}\,d_\alpha\right) \text{(diffusion)} \quad (9b)$$

If a μ can be found to satisfy *Eq. 9a* in the voxel indexed by (i,j,k), the "reaction" was a reaction; otherwise, the "reaction" will satisfy *Eq. 9b* for some α and be a diffusion out of the voxel indexed by (i,j,k).

Hence, we can outline the stochastic numerical simulation algorithm.

1) Initialization: initialize all relative variables, including calculating the "reaction rates" for all "reactions" in all voxels, and the initial numbers of molecules in all voxels. Calculate the variable h_μ, d_α in each voxel and calculate a as defined above. Also set initial time $t = 0$.

2) Advance the simulation and update the system states: first, generate one pair of random numbers (r_1, r_2), calculate τ, and determine the $(ijk)_{th}$ voxel where the "reaction" R_μ occurs; second, advance t by τ and update the numbers of molecules of those species involved in "reaction" R_μ in the $(ijk)_{th}$ voxel (note: if it is a diffusion, the quantity of the corresponding molecules in the appropriate neighboring voxel, where the molecules diffuse also has to be updated). Finally, recalculate the variable a based on the new quantities of molecules in the relevant voxels.

3) If t does not reach the ending point, write out t and the molecule quantities of interest and return to step 2; if t reaches the ending point or all molecules have vanished, terminate the simulation.

The method only requires two random numbers for each time step; hence the computation for random number generation encountered in traditional simulations is reduced dramatically. This allows the simulation to include a large number of subvolumes (voxels) for more realistic models.

To verify that the model was working properly, results were compared with those obtained with a mixed stochastic-deterministic model described earlier (Holmes 2000).

Dendritic spine model

The dendritic spine model used here is extended from that used previously (Holmes 2000). Taking into account calcium diffusion, pumping, and binding to buffers, this model calculates spine head calcium concentration after calcium influx through NMDA receptor channels. The spine head is chosen to be of long-thin type. The spine head is a $0.5 \times 0.5 \times 0.55$-$\mu$m rectangular box, and the spine neck is a $0.1 \times 0.1 \times 0.8$-$\mu$m rectangular box, connecting to the underlying dendrite, which is represented by a $2 \times 1 \times 1$-μm rectangular box. Because CaMKII and calcineurin molecules are mostly localized within the outer 50 nm of the spine head, the outermost layer of the spine head is filled with $50 \times 50 \times 50$-nm voxels, and the rest of the spine head is filled with $0.1 \times 0.1 \times 0.1$-$\mu$m voxels. There are a total of 225 voxels in the spine head. The spine neck is divided into 8 $0.1 \times 0.1 \times 0.1$-$\mu$m voxels, and the underlying dendrite is divided into 16 $0.5 \times 0.5 \times 0.5$-$\mu$m voxels.

In the spine, calcium influx through NMDA receptor channels enters the spine head uniformly through the middle 16 voxels in the outer layer of the spine head, representing the region of the postsynaptic density. Calcium can bind to calbindin or calmodulin, and calmodulin with zero to four calcium ions bound can bind to CaMKII, calcineurin, or neurogranin. Calcium and calmodulin can diffuse freely, but CaMKII and calcineurin are restricted to the outermost layer of the spine head. There are 83 CaMKII holoenzymes (each with 2 rings of 6 subunits each) and 200 calcineurin molecules whose primary function in these short simulations is to compete with CaMKII for calmodulin. Neurogranin is present in all areas of the spine and dendrite with a total concentration of 26.7 μM. Total calbindin concentration is 40 μM, and total calmodulin concentration is 13.3 μM. Recently CaMKII was shown to be activated by calmodulin having only two bound Ca^{2+} ions (Shifman et al. 2006); therefore in the model, a CaMKII subunit bound with $CaMCa_x$, where x is ≥ 2 is considered to be in the "bound" state. A bound subunit can become autophosphorylated and reach the "trapped" state ($CaMCa_x$ bound and phosphorylated) only if its immediate neighbor on the same ring of the CaMKII holoenzyme is also in the bound or trapped state (or with lower probability, in the autonomous or capped states). If a trapped subunit loses $CaMCa_x$, it is considered to be in the autonomous state and, from there, autophosphorylation can occur in the calmodulin binding site to bring the subunit into the "capped" state if the neighboring subunit in the holoenzyme ring to the right or left is bound, trapped, autonomous, or capped.

RATE CONSTANT DETAILS. The two calcium buffers in the model are calbindin and calmodulin. The concentration of calbindin in adult dentate granule cells has been estimated to be 40 μM (Müller et al. 2005) and that is the concentration used in the model. Calbindin can bind four Ca^{2+} ions; two sites are high affinity sites and two are low affinity. On and off rates in the model were 5.5 $\mu M^{-1}\ s^{-1}$ and 2.6 s^{-1} for the high-affinity site and 43.5 $\mu M^{-1}\ s^{-1}$ and 35.8 s^{-1} for the low-affinity site (Nagerl et al. 2000; with modification of on rates suggested by Berggard et al. 2002). Calmodulin also binds four Ca^{2+} ions, two on the N-lobe and two on the C-lobe. The K_d values used were 10 and 1.2 μM for the C-lobe and 50 and 10 μM for the N-lobe (Linse et al. 1991). The on and off rates are shown in the back frames of Fig. 1, *A–C*. Dissociation rates are based on data from Gaertner et al. (2004) and, together with the K_d values, these determined the on rates. Diffusion coefficients were 0.223 for calcium (Allbritton et al. 1992), 0.0223 for calmodulin (Schmidt et al. 2007), and 0.02 for calbindin (Schmidt et al. 2005) (all in units of μm^2/ms). Most of the calmodulin is bound to neurogranin at rest.

Rate constants for Ca^{2+} binding to $CaMKIICaMCa_x$ and $CaMCa_x$ binding to CaMKII are given in Fig. 1*A*. For Ca^{2+} binding to $CaMKIICaMCa_x$, the dissociation rates are from Gaertner et al. (2004); the K_d values were assumed to be 10-fold higher affinity than calcium binding to $CaMCa_x$ without the kinase, and the on rates were computed from the K_d and the off rates. These rates are shown in the front frame of Fig. 1*A*. For $CaMCa_x$ binding to CaMKII, the K_d and dissociation rate for $CaMCa_4$ binding to CaMKII are based on values from Meyer et al. (1992). The other values on the slanted lines in the figure are computed from thermodynamic considerations, given the remaining rate constants.

Rate constants for Ca^{2+} binding to calcineurin bound with $CaMCa_x$ and $CaMCa_x$ binding to calcineurin (CaN) are given in Fig. 1*B*. For Ca^{2+} binding to $CaNCaMCa_x$, the K_d values of 0.1, 0.06, 0.3, and 0.08 μM were taken from Stemmer and Klee (1994). The on and off rates were assumed to be in the same range as those with CaMKII. These rates are shown in the front frame of Fig. 1*B*. For $CaMCa_x$ binding to CaN, the K_d and on and off rates for $CaMCa_4$ binding to CaN were taken from Quintana et al. (2005). The other values on the slanted lines in this figure are computed from thermodynamic considerations, given the other rate constants.

Rate constants for Ca^{2+} binding to neurogranin bound with $CaMCa_x$ and $CaMCa_x$ binding to neurogranin (Ng) are given in Fig. 1*C*. For Ca^{2+} binding to Ng-$CaMCa_x$, the dissociation rates were taken from Gaertner et al. (2004) and the on rates were assumed to be the same as calcium binding to calmodulin without neurogranin. These rates are shown in the front frame of Fig. 1*C*. For $CaMCa_x$ binding to Ng, we assumed that CaM binding to Ng had a K_d of 3 μM (reports range 1–5 μM; see Zhabotinsky et al. 2006). The on and off rates were chosen from thermodynamic considerations but were similar to those in Kubota et al. (2007).

CaMKII subunits in the bound state as defined above can become trapped or phosphorylated if a neighboring subunit on the same ring of the holoenzyme is also bound, trapped, and with 0.4 times lower probability, autonomous or capped. The trapping rate constant is 10 s^{-1}, which is much higher than in our previous models but seems more consistent with data from Bradshaw et al. (2003). We do not model dephosphorylation in detail here; the rate used is 0.003 s^{-1}, making this a rare event within the limited time course of the results shown. Subunits in the trapped state can gain or lose Ca^{2+} ions. Our rate constants for this are given in the back frame of Fig. 1*D*. The dissociation rates were taken from Gaertner et al. (2004), and the association rates were chosen to make the K_d of each step the same as with the unphosphorylated kinase. Rate constants for the transition from trapped states to the autonomous state are also shown. Rates were chosen to be consistent with Meyer et al. (1992) (Fig. 3), although these reactions were not common within the time course of the current simulations.

RESULTS

Combined effect of two kinds of noise

We first studied the combined effect of noise from both stochastic opening of NMDA receptor channels and stochastic CaMKII activation. Opening of NMDA receptor channels at the synapse of interest was modeled stochastically with MCell v. 2.50 (Stiles and Bartol 2001), and CaMKII activation within the dendritic spine was also simulated stochastically. Opening of NMDA receptor channels on other synapses was modeled deterministically. An eight-pulse tetanus at 100 Hz was applied to 300 synapses in a model of a dentate granule cell to determine the voltage change at the synapses. At each synapse, each pulse in the tetanus was modeled as the release of 2,000 glutamate molecules. Each deterministic synapse had 63 AMPA and 14 NMDA receptor channels. The stochastic synapse had 63 AMPA receptors and 10–26 NMDA receptors depending on the simulation trial group. We used MCell results together with the voltage from the neuron level model to generate 30 trials of calcium signals, which were used in the spine model to compute levels of CaMKII activation. In the 30

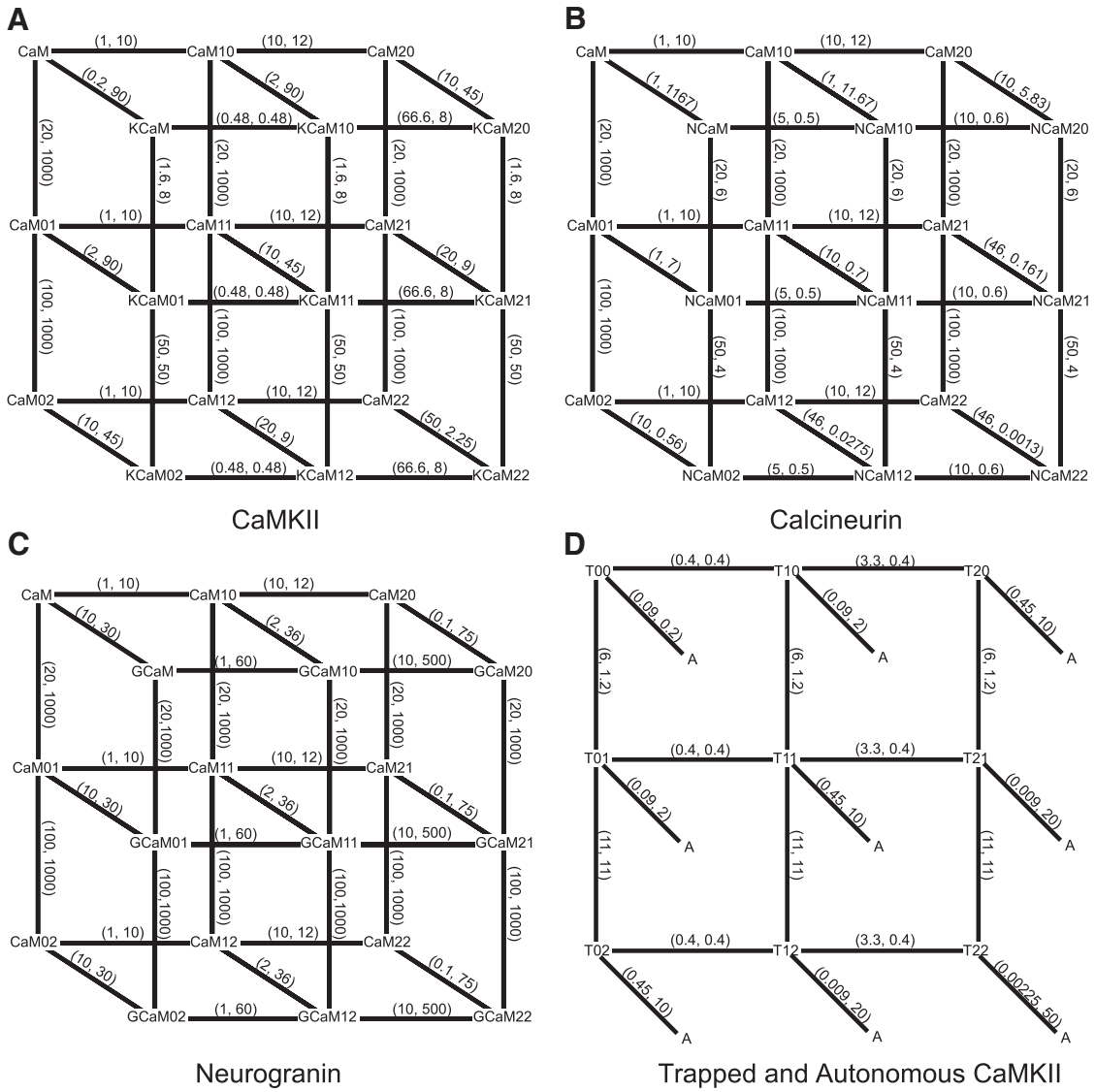

FIG. 1. Reaction schemes and rate constants used in the simulations. *A*: calcium-calmodulin dependent protein kinase II (CaMKII) reactions. The back frame is calcium binding to calmodulin. Calmodulin with calcium bound is represented as CaMij, where i and j are the number of calcium ions bound to the C-lobe and N-lobe, respectively. KCaMij represents CaMKII bound with CaMij. Numbers in parentheses represent the forward and backward rate constants for the given reaction. *B*: calcineurin reactions. NCaMij represents calcineurin bound with CaMij. The calcium binding to calmodulin reactions are again depicted in the back frame. *C*: neurogranin reactions. GCaMij is neurogranin bound with CaMij. *D*: reactions associated with trapped and autonomous CaMKII subunits. Tij represents a phosphorylated subunit that has "trapped" calmodulin bound with i C-lobe calcium ions and j N-lobe calcium ions. A is the phosphorylated CaMKII subunit with no CaM bound. Other reactions not shown here schematically are described in the text. Rate constants in $\mu M^{-1}\ s^{-1}$ or s^{-1}.

trials, all of the simulation conditions were the same, including the locations of the NMDA receptors, AMPA receptors, and glutamate uptake transporters, except that different random seeds were used in all MCell and stochastic CaMKII activation simulations.

The number of NMDA receptor channel openings computed stochastically with MCell after an eight-pulse, 100-Hz tetanus showed considerable variability across trials as shown in Fig. 2. Trials with maximal opening and minimal opening, representing extreme cases encountered among 30 trials when there were 19 NMDA receptors at the synapse, are compared in Fig. 2*A*. In Fig. 2*A* (*top*), the peak number of open NMDA channels was eight, and there were long stretches when there were always one or two open channels. In Fig. 2*A* (*middle*), the peak number of open channels was three, and stretches where there was at least one open channel were comparatively short. NMDA receptor channels that reach the open state are subject to voltage-dependent magnesium block. Taking into account the voltage computed in the neuron level model, the peak number of open and unblocked channels was three and two for these two trials, respectively, as shown in Fig. 2*B* (*top* and *middle*). The bottom traces in Fig. 2 show the average number of open NMDA channels both with and without magnesium block. These traces show some late channel openings commonly seen in these trials. We sometimes saw isolated openings 900–1,000 ms after the tetanus.

The variability in the number of open and unblocked NMDA receptor channels translated into very different calcium signals in the outer layer of the dendritic spine head as shown in Fig. 3*A*. Here we show the calcium concentration for the two extreme cases from Fig. 2 and, for comparison, the calcium concentration averaged over all 30 trials. The large difference in calcium

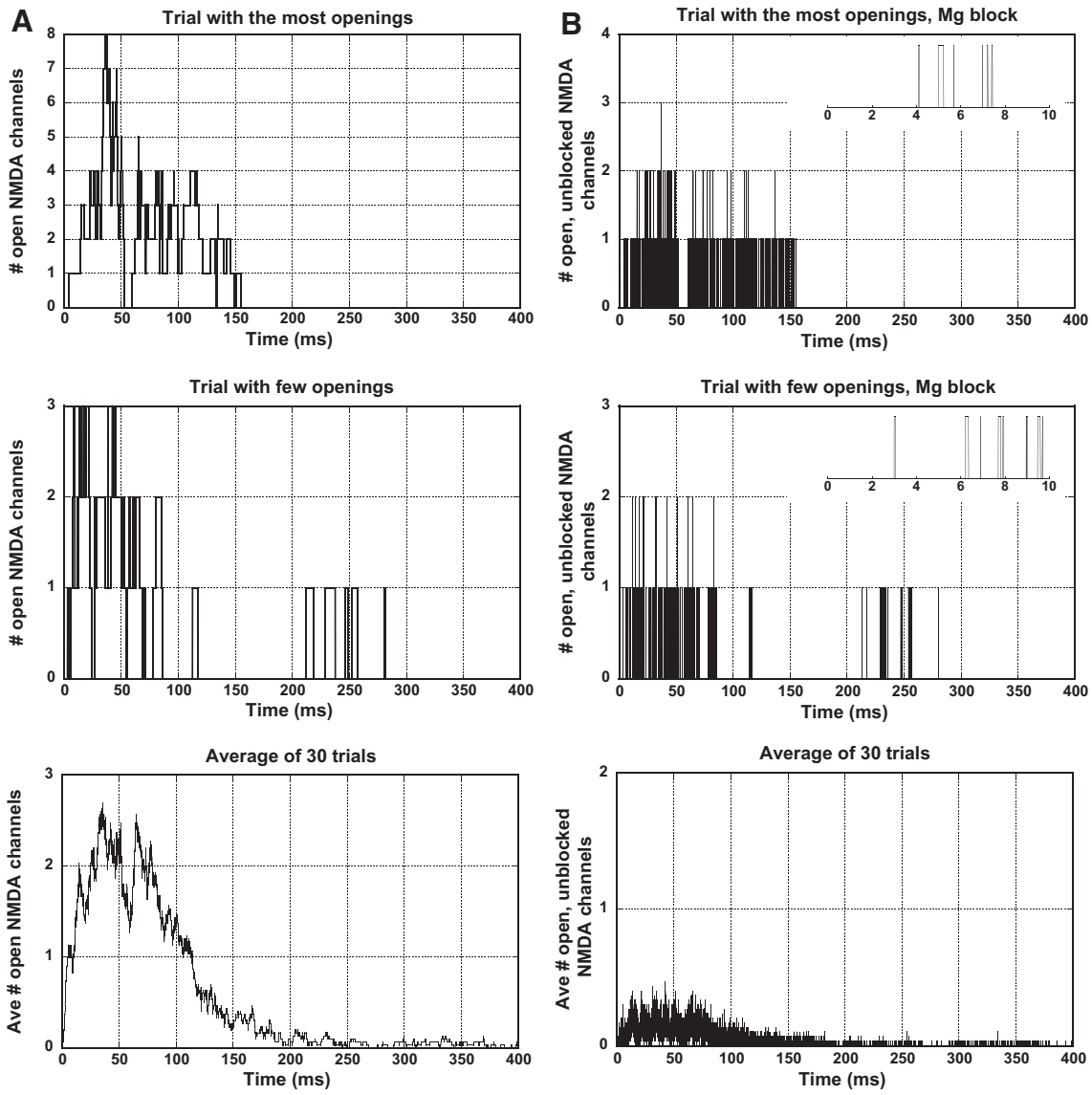

FIG. 2. Number of open *N*-methyl-D-aspartate (NMDA) receptors in response to an 8-pulse 100-Hz tetanus. *A*: examples of extreme cases among 30 trials computed with MCell and the average of 30 trials. *B*: NMDA receptor channel openings after taking into account voltage-dependent magnesium block. *Insets*: magnification of the first 10 ms of the traces to show the number of open, unblocked channels more clearly. Results are shown for the extreme cases and the average of 30 trials. In all cases, there were 19 NMDA receptors and 63 AMPA receptors at the synapse.

concentration was expected because total calcium influx varied over a two- to threefold range among the pictured trials (11,000–26,000 Ca^{2+} ions). This difference in the calcium signal caused a huge difference in the number of activated CaMKII subunits, as shown in Fig. 3*B*. Results from all 30 trials, as well as the average, are shown in this figure, and they show that the two extreme cases from Fig. 2 are not isolated examples but reflect the inherent variability in CaMKII activation.

Because the induction of LTP is known to require a high-frequency tetanus, we next sought to examine the variability in CaMKII activation for different tetanus frequencies. We produced plots of CaMKII activation similar to Fig. 3*B* for 10- to 400-Hz stimulation, which are summarized in Fig. 4*A*. These results again show that the effect of noise on CaMKII activation can be substantial. Perhaps surprisingly, a large number of activated CaMKII subunits occurred for two 20-Hz trials, and some small numbers of activated subunits occurred in some 100-Hz trials. The variability among the 20-Hz trials and their time courses are pictured in Fig. 4*B*. Nevertheless, the mean and median number of activated CaMKII subunits generally increased with frequency in the expected manner for 10–100 Hz. The illustrated example shows a dip for 200- and 400-Hz tetani trial groups, but this was not a consistent finding; results with 18 NMDA receptors at the synapse showed constant means and medians for 100- to 400-Hz trial groups.

NMDA receptor number provides an additional source of variability

To this point, the illustrated simulations always used 19 NMDA receptors at the stochastic synapse. How would small changes in the number of NMDA receptors at the synapse affect CaMKII activation? To answer this, we used eight-pulse 20- and 100-Hz

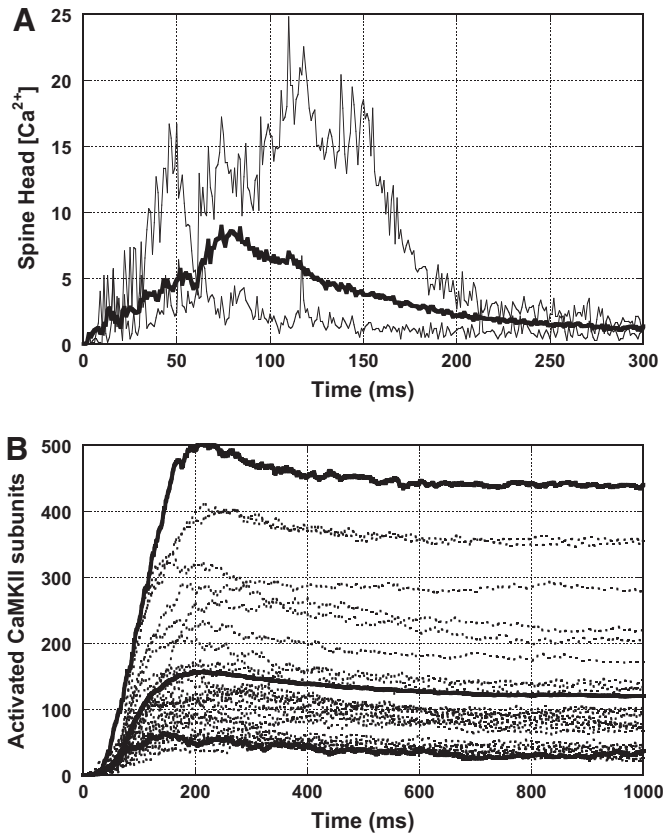

FIG. 3. Variability in calcium concentration and CaMKII activation among trials is large. *A*: calcium concentration in the spine head for the extreme cases from Fig. 2 (thin solid lines) and the average of 30 trials (thick solid line). *B*: CaMKII activation (total number of bound, trapped, autonomous, and capped subunits) for all 30 trials. Solid lines represent the most extreme cases and the average. Units in A are μM.

tetani with different numbers of NMDA receptor channels to generate the input calcium signals, and then we computed CaMKII activation. We simulated 30 trials each for 10–26 NMDA receptor channels at each tetanus frequency.

We found that, although the general trend, as expected, was that more CaMKII subunits were activated as the number of NMDA receptor channels or the tetanus frequency was increased, there was considerable variability among runs as shown in Fig. 5, *A* and *B*. Means and medians only are plotted in Fig. 5*C* to show trends more clearly. In the 100-Hz tetanus results, the mean number of activated CaMKII subunits increased fourfold and the median increased threefold as the number of NMDA receptors was raised from 14 to 18; the mean increased another twofold and the median threefold as the number of NMDA receptors was raised from 18 to 24. In the 20-Hz tetanus results, increases in the number of activated CaMKII subunits with increasing NMDA receptor number were much more gradual; nevertheless, there were a number of trials at this tetanus frequency at nearly every NMDA receptor number where CaMKII activation exceeded the corresponding mean or median at 100 Hz.

Individual effect of two kinds of noises

How much of the observed variability comes from stochastic opening of NMDA receptor channels and how much comes from stochastic CaMKII activation reactions? We computed the calcium influx generated by an eight-pluse 100-Hz tetanus at a synapse with 19 NMDA receptor channels and used this same calcium signal in the dendritic spine model but with different random seeds for the CaMKII activation reactions. The calcium signal chosen was the trial that had calcium influx closest to the mean of 30 trials. The results suggest that CaMKII reactions provide a much smaller source of variability than NMDA receptor channel openings (Fig. 6).

We next sought to quantify this result and extend it to include the effect of different numbers of NMDA receptors at the synapse. To quantify the combined effect of both types of noise on CaMKII activation variability, we first measured the relative fluctuation $\sqrt{<(N - <N>)^2>}/<N>$ of the total number of activated CaMKII subunits, where N is the sum of the number of bound, trapped, autonomous, and capped subunits in each trial at 1 s and $<N>$ is the average over 30 trials. To separate the two sources of noise, we compared results computed with stochastic models of NMDA receptor channel openings and a stochastic model of CaMKII activation to results computed, as for Fig. 6, with the trial whose NMDA receptor channel openings and subsequent calcium influx was closest to the mean of 30 trials and stochastic models of CaMKII activation. This was done for NMDA receptor numbers of 12–26. Results are shown in Fig. 7.

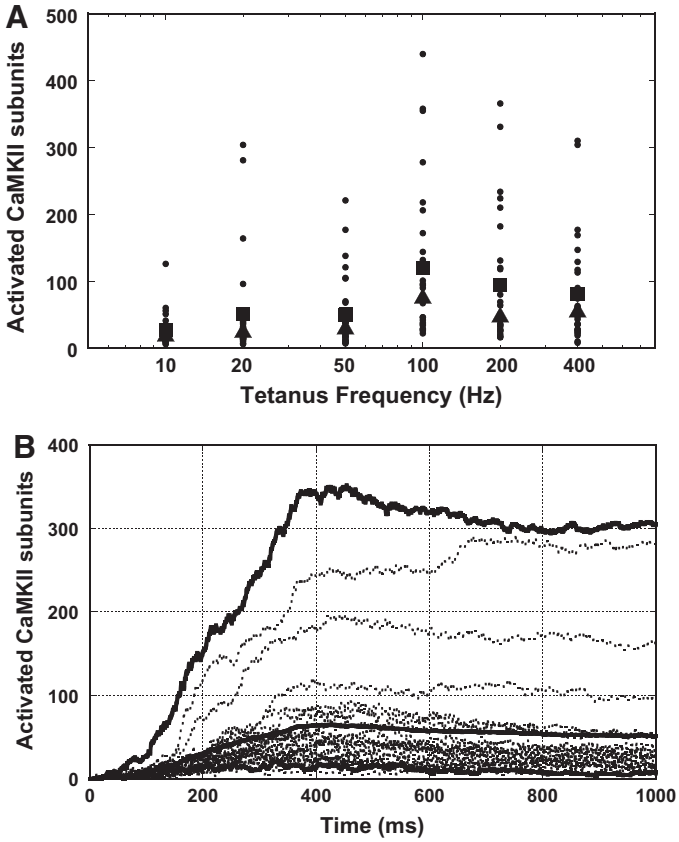

FIG. 4. CaMKII activation for different tetanus frequencies. *A*: the number of activated subunits (total number of bound, trapped, autonomous, and capped subunits) at 1 s for each of 30 trials at each tetanus frequency (small dots), together with the mean (squares) and medians (triangles) for each frequency. *B*: results for the 8-pulse, 20-Hz tetanus showing the time course of CaMKII activation for all 30 trials. In all cases, there were 19 NMDA receptors and 63 AMPA receptors at the synapse.

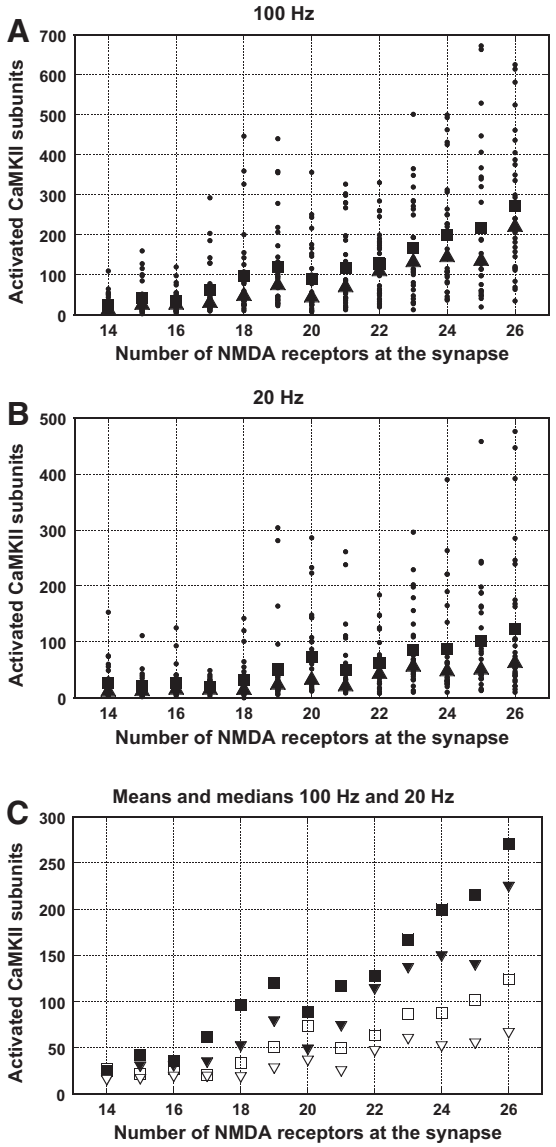

FIG. 5. Number of activated CaMKII subunits at 1 s as a function of the number of NMDA receptor channels at the synapse for different tetanus frequencies. Small dots represent individual trials. Means and medians are squares and triangles, respectively. *A*: 100-Hz tetanus. *B*: 20-Hz tetanus. *C*: means and medians for 100- (solid square and triangle) and 20-Hz tetanus (open squares and triangles) are shown together.

We see from Fig. 7 that the relative fluctuation of the number of activated CaMKII subunits attributed to stochastic CaMKII activation alone is just 12–28% of that coming from both stochastic opening of NMDA receptor channels and stochastic CaMKII activation, with the percentages being 12–15% for larger numbers of NMDA receptors. This was to be expected because, in the spine head, there are more CaMKII subunits (~1,000 in these simulations) than NMDA receptor channels (~20). As the number of NMDA receptor channels was increased, the relative fluctuation in the number of activated CaMKII subunits decreased. For example, when NMDA receptor channel number was 12, the relative fluctuation from stochastic opening of NMDA receptor channels and stochastic CaMKII reactions was 110%; however, when receptor number was 26, the relative fluctuation was reduced to 60%. Similarly, the relative fluctuation when only CaMKII reactions were

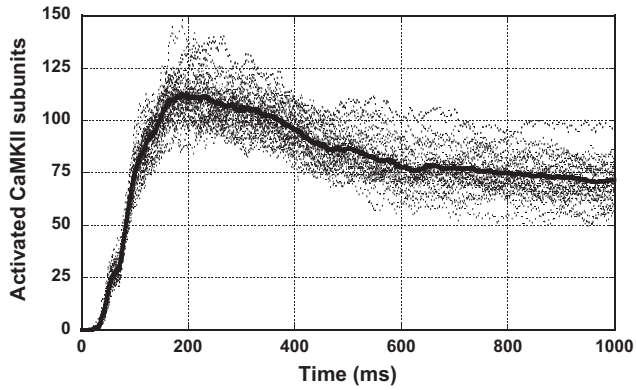

FIG. 6. Variability in CaMKII activation from CaMKII kinetics alone is relatively small. The same calcium influx function (from the trial that provided calcium influx closest to the mean of 30 trials) was used as input to stochastic simulations of CaMKII activation initiated with different random seeds. Dotted lines show results for 30 individual trials. Solid line is the average of the 30 trials; 100-Hz tetanus and 19 NMDA receptors.

modeled stochastically dropped from 22 to 8% over the same span of NMDA receptor number. One reason for this phenomenon is that increasing the number of NMDA receptor channels will decrease the fluctuation of the number of open NMDA receptor channels, which decreases the fluctuation of calcium influx, resulting in a decrease in the fluctuation in the number of activated CaMKII subunits. We note that the total number of activated CaMKII subunits in these simulations was low compared with the number of available subunits, especially when the number of NMDA receptors was small. This contributed to the high relative fluctuation shown in Fig. 7. As the number of NMDA receptor channels was increased and the number of activated CaMKII subunits became significant relative to the total number of subunits, the fluctuation naturally decreased.

DISCUSSION

It is well accepted that CaMKII activation is necessary and sufficient to induce some forms of LTP (Hayashi et al. 2000; Lledo et al. 1995). CaMKII activation occurs as a series of complicated stochastic processes, and there are a number of

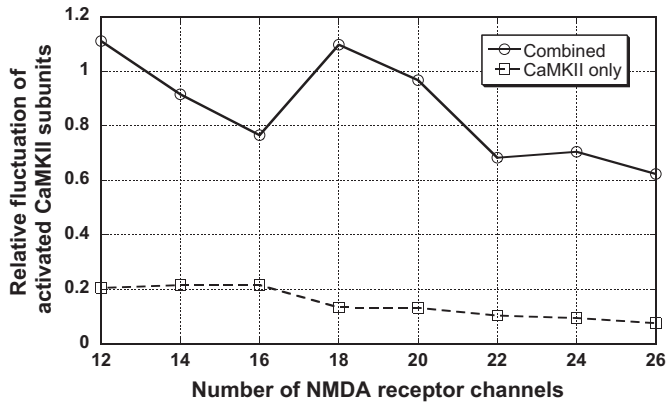

FIG. 7. Relative fluctuation of the number of activated CaMKII subunits as a function of the number of NMDA receptor channels. Solid line, the combined effects of 2 kinds of noise; dashed line, the effect of stochastic CaMKII activation kinetics alone; the calcium influx function was the trial that produced calcium influx closest to the mean of 30 trials for the indicated number of NMDA receptors; different seeds were used in 30 stochastic CaMKII reaction simulations.

sources contributing to CaMKII activation variability within a dendritic spine (Chen et al. 1999; Franks and Sejnowski 2004; Rosenmund et al. 1995; Santucci and Raghavachari 2008; Xia and Storm 2005). Here we combine a fully stochastic synapse level model with a neuron level model and a fully stochastic model of reaction-diffusion within a dendritic spine to focus on two sources of noise: stochastic opening of NMDA receptor channels and stochastic CaMKII activation within a dendritic spine. Our results show that noise has important effects on CaMKII activation variability. Of the two sources of noise examined here, noise involved with stochastic opening of NMDA receptor channels was 5–10 times more important than noise in stochastic CaMKII activation reactions. The reason for this is that there are many more CaMKII subunits than NMDA receptor channels. Here we had ~1,000 CaMKII subunits (83 holoenzymes) in one dendritic spine compared with ~10–20 NMDA receptor channels (Racca et al. 2000). According to the square root law of statistical theory, the precision of the sample mean improves with the square root of the sample size. Applying the numbers given above, we would expect that the variability in CaMKII activation should be the square root of 1000/20 or 7 times larger from the stochastic opening of NMDA receptor channels than from stochastic CaMKII activation kinetics. This is exactly the relationship we obtained in the simulations when NMDA receptor number was 18 or larger. With smaller NMDA receptor numbers, the ratio we found fell to 3–5, mostly likely the result of having very few CaMKII subunits becoming activated in these cases. We want to note that, in early simulations in which we excluded calbindin, a larger fraction of the CaMKII subunits became activated for all numbers of NMDA receptors as would be expected; qualitative results were similar to those shown, and the expected sevenfold relationship was also found. If the number of holoenzymes was much less than that used in the model, say 30, then following the above formula, we would expect variability in CaMKII activation to be only 4 times larger from stochastic opening of NMDA receptor channels than from stochastic CaMKII activation kinetics. In this case, fluctuation because of CaMKII activation kinetics would become more important, but fluctuation because of stochastic NMDA channel openings would still dominate.

There are many sources of noise that we have not explored in this study. These can be divided into *1*) additional factors to be considered and *2*) variations in parameter values chosen. Additional factors to be considered include variations or heterogeneity in receptor type (i.e., NR1/2A vs. NR1/2B) (Chen et al. 1999; Santucci and Raghavachari 2008), nonuniform probability of vesicle release (Hanse and Gustafsson 2001; Rosenmund et al. 1993), stochasticity in other CaMKII activation reactions, particularly gating of phosphatase activation/deactivation (Bhalla 2002a,b); variation in spine shape (Holmes 1990; Schmidt and Eilers 2009), variation in the site of vesicle release (Uteshev and Pennefather 1997), variation in the location of NMDA receptors in the PSD (Santucci and Raghavachari 2008), and variation with the use of different proposed NMDA kinetic reaction schemes (Banke and Traynelis 2003; Popescu and Auerbach 2003; Yuan et al. 2005). As for parameter values, possible sources of variability include: the number of CaMKII holoenzymes in the spine head (Peterson et al. 2003), the diffusion rate of glutamate in the cleft (Holmes 1995; Rusakov and Kullmann 1998; Ventriglia and Maio 2000), the diffusion rate of calcium inside the spine, glutamate uptake rates, calcium pump rates, number of glutamate molecules in a vesicle (Burger et al. 1989; Holmes 1995; Riveros et al. 1986) and synaptic cleft width (Rusakov and Kullmann 1998; Ventriglia and Maio 2000). We suspect that noise from these sources will be less than that from stochastic variations in NMDA receptor channel openings, but verification of this awaits future work.

What are the consequences of noise for LTP induction and learning and memory? Because of noise in NMDA receptor channel openings, it may be necessary to repeat a tetanus or have repeated short bursts of stimulation to reliably kick CaMKII activation to a high level (Li and Holmes 2000). This may be particularly important during development when the number of NMDA receptors at a synapse may be small, making variability of CaMKII activation large. Only those synapses that receive repeated stimulation or certain patterned stimulation can reliably overcome the effects of noise. In addition, calcium influx is very sensitive to the number of NMDA receptors at the synapse and the peak number of open NMDA receptor channels is small (Dalby and Mody 2003; Nimchinsky et al. 2004). Although the number of NMDA receptor channels at synapses has been found to be far less variable than the number of AMPA receptor channels (Takumi et al. 1999), the results here show that even small differences in the number of NMDA receptor channels per synapse can have large effects on CaMKII activation. With physiological patterns of stimulation, noise may allow the calcium signal to exceed threshold for CaMKII activation when it would not do so otherwise. Noise may be an essential feature for selecting synapses to undergo potentiation. It is worth noting that a noise-driven stochastic selection mechanism for potentiating synapses has been found optimal for storing multiple memories in network models (Fusi 2002).

ACKNOWLEDGMENTS

We thank L. M. Grover and J. Ambros-Ingerson for comments and suggestions on drafts of this manuscript. We acknowledge the work of Y. Li during early stages of this project through 2003 and also thank N. Desmond for the morphology of the dentate granule cell used in the simulations.

GRANTS

This work was supported by National Institute on Alcohol Abuse and Alcoholism Grant AA-14294 via the Collaborative Research in Computational Neuroscience program and by the Scientific Research Fund of the Hunan Provincial Education Department (07B075).

REFERENCES

Allbritton NL, Meyer T, Streyer L. Range of messenger action of calcium ion and inositol 1,4,5-trisphosphate. *Science* 258: 1812–1815, 1992.

Ascher P, Nowak L. The role of divalent cations in the N-methyl-D-aspartate responses of mouse central neurones in culture. *J Physiol* 399: 247–266, 1988.

Banke TG, Traynelis SF. Activation of NR1/NR2B NMDA receptors. *Nat Neurosci* 6: 144–152, 2003.

Berggard T, Szczepankiewicz O, Thulin E, Linse S. Myo-inositol monophosphatase is an activated target of calbindin D28k. *J Biol Chem* 277: 41954–41959, 2002.

Bezrukov SM, Vodyanoy I. Noise-induced enhancement of signal transduction across voltage-dependent ion channels. *Nature* 378: 362–364, 1995.

Bhalla US. Biochemical signaling networks decode temporal patterns of synaptic input. *J Comput Neurosci* 13: 49–52, 2002a.

Bhalla US. Mechanisms for temporal tuning and filtering by postsynaptic signaling pathways. *Biophys J* 83: 740–752, 2002b.

Bhalla US. Signaling in small subcellular volumes. I. Stochastic and diffusion effects on individual pathways. *Biophys J* 87: 733–744, 2004a.

Bhalla US. Signaling in small subcellular volumes. II. Stochastic and diffusion effects on synaptic network properties. *Biophys J* 87: 745–753, 2004b.

Bliss TVP, Collingridge GL. A synaptic model of memory: long-term potentiation in the hippocampus. *Nature* 361: 31–39, 1993.

Bradshaw JM, Kubota Y, Meyer T, Schulman H. An ultrasensitive Ca^{2+}/calmodulin-dependent protein kinase II–protein phosphatase 1 switch facilitates specificity in postsynaptic calcium signaling. *Proc Natl Acad Sci USA* 100: 10512–10517, 2003.

Burger PM, Mehl E, Cameron PL, Maycox PR, Baumert M, Lottspeich F, DeCamilli P, Jahn R. Synaptic vesicles immunoisolated from rat cerebral cortex contain high levels of glutamate. *Neuron* 3: 715–720, 1989.

Byrne MJ, Putkey JA, Waxham NM, Kubota Y. Dissecting cooperative calmodulin binding to CaM kinase II: a detailed stochastic model. *J Comput Neurosci* 27: 621–638, 2009.

Calvin WH, Stevens CF. Synaptic noise as a source of variability in the interval between action potentials. *Science* 155: 842–844, 1967.

Chen N, Luo T, Raymond LA. Subtype-dependence of NMDA receptor channel open probability. *J Neurosci* 19: 6844–6854, 1999.

Clay JR, DeFelice LJ. Relationship between membrane excitability and single channel open-close kinetics. *Biophys J* 42: 151–157, 1983.

Coomber C. Current theories of neuronal information processing performed by Ca^{2+}/calmodulin-dependent protein kinase II with support and insights from computer modeling and simulation. *Comput Chem* 22: 251–263, 1998.

Cossart R, Epsztein J, Tyzio R, Becq H, Hirsch J, Ben-Ari Y, Crépel V. Quantal release of glutamate generates pure kainate and mixed AMPA/Kainate EPSCs in hippocampal neurons. *Neuron* 13: 1385–1393, 1994.

Dalby NO, Mody I. Activation of NMDA receptors in rat dentate gyrus granule cells by spontaneous and evoked transmitter release. *J Neurophysiol* 90: 786–797, 2003.

Dosemeci A, Albers RW. A mechanism for synaptic frequency detection through autophosphorylation of CaM kinase II. *Biophys J* 70: 2493–2501, 1996.

Enslen H, Soderling TR. Roles of calmodulin-dependent protein kinases and phosphatase in calcium-dependent transcription of immediate early genes. *J Biol Chem* 269: 20872–20877, 1994.

Ermentrout GB, Galan RF, Urban NN. Reliability, synchrony and noise. *Trends Neurosci* 34: 428–434, 2008.

Faisal AA, Laughlin SB. Stochastic simulations on the reliability of action potential propagation in thin axons. *PLoS Comput Biol* 3: e79, 2007.

Faisal AA, Selen LP, Wolpert DM. Noise in the nervous system. *Nat Rev Neurosci* 9: 292–303, 2008.

Fellous JM, Rudolph M, Destexhe A, Sejnowski TJ. Synaptic background noise controls the input/output characteristics of single cells in an in vitro model of in vivo activity. *Neuroscience* 122: 811–829, 2003.

Franks KM, Sejnowski TJ. Complexity of calcium signaling in synaptic spines. *Bioessays* 24: 1130–1144, 2004.

Franks KM, Stevens CF, Sejnowski TJ. Independent sources of quantal variability at single glutamatergic synapses. *J Neurosci* 23: 3186–3195, 2003.

Fukunaga K, Muller D, Miyamoto E. CaM kinase II in long-term potentiation. *Neurochem Int* 28: 343–358, 1996.

Fukunaga K, Stoppini L, Miyamoto E, Muller D. Long term potentiation is associated with an increased activity of Ca^{2+}/calmodulin-dependent protein kinase II. *J Biol Chem* 268: 7863–7867, 1993.

Fusi S. Hebbian spike-driven synaptic plasticity for learning patterns of mean firing rates. *Biol Cybern* 87: 459–470, 2002.

Gaertner TR, Putkey JA, Waxham MN. RC3/Neurogranin and Ca^{2+}/calmodulin-dependent protein kinase II produce opposing effects on the affinity of calmodulin for calcium. *J Biol Chem* 279: 39374–39382, 2004.

Gillespie DT. A general method for numerically simulating the stochastic time evolution of coupled chemical reactions. *J Comput Phys* 22: 403–434, 1976.

Gillespie DT. Concerning the validity of the stochastic approach to chemical kinetics. *J Stat Phys* 16: 311–318, 1977.

Graupner M, Brunel N, Friston KJ. STDP in a bistable synapse model based on CaMKII and associated signaling pathways. *PLoS Comput Biol* 3: e221, 2007.

Hanse E, Gustafsson B. Vesicle release probability and pre-primed pool at glutamatergic synapses in area CA1 of the rat neonatal hippocampus. *J Physiol* 531: 481–493, 2001.

Hayashi Y, Shi SH, Esteban JA, Piccini A, Poncer JC, Malinow R. Driving AMPA receptors into synapses by LTP and CaMKII: requirement for GluR1 and PDZ domain interaction. *Science* 287: 2262–2267, 2000.

Hayer A, Bhalla US. Molecular switches at the synapse emerge from receptor and kinase traffic. *PLoS Comput Biol* 1: e20, 2005.

Hoch T, Wenning G, Obermaver K. Optimal noise-aided signal transmission through populations of neurons. *Phys Rev E* 68: 011911–011921, 2003.

Holmes WR. Is the function of dendritic spines to concentrate calcium? *Brain Res* 519: 338–342, 1990.

Holmes WR. Modeling the effect of glutamate diffusion and uptake on NMDA and non-NMDA receptor saturation. *Biophys J* 69: 1734–1747, 1995.

Holmes WR. Models of calmodulin trapping and CaM Kinase II activation in a dendritic spine. *J Comput Neurosci* 8: 65–85, 2000.

Holmes WR, Levy WB. Insights into associative long-term potentiation from computational models of NMDA receptor-mediated calcium influx and intercellular calcium concentration changes. *J Neurophysiol* 63: 1148–1168, 1990.

Holmes WR, Levy WB. Quantifying the role of inhibition in associative long-term potentiation in dentate granule cells with computational models. *J Neurophysiol* 78: 103–116, 1997.

Jaramillo F, Wiesenfeld K. Mechanoelectrical transduction assisted by Brownian motion: a role for noise in the auditory system. *Nat Neurosci* 1: 384–388, 1998.

Johnson HA. Thermal noise and biological information. *Q Rev Biol* 62: 141–152, 1987.

Keller DX, Franks KM, Bartol TM, Sejnowski TJ. Calmodulin activation by calcium transients in the postsynaptic density of dendritic spines. *PLoS ONE* 3: e2045, 2008.

Kubota Y, Bower JM. Transient versus asymptotic dynamics of CaM Kinase II: possible roles of phosphatase. *J Comput Neurosci* 11: 263–279, 2001.

Kubota Y, Putkey JA, Waxham MN. Neurogranin controls the spatiotemporal pattern of postsynaptic Ca^{2+}/CaM signaling. *Biophys J* 93: 3848–3859, 2007.

Leranth C, Petnehazy O, MacLusky NJ. Gonadal hormones affect spine synaptic density in the ca1 hippocampal subfield of male rats. *J Neurosci* 23: 1588–1592, 2003.

Li Y, Holmes WR. Comparison of CaMKinase II activation in a dendritic spine computed with deterministic and stochastic models of the NMDA synaptic conductance. *Neurocomputing* 32–33: 1–7, 2000.

Linse S, Helmersson A, Forsen S. Calcium binding to calmodulin and its globular domains. *J Biol Chem* 266: 8050–8054, 1991.

Lisman J. Long-term potentiation: outstanding questions and attempted synthesis. *Philos Trans R Soc Lond B Biol Sci* 358: 829–842, 2003.

Lisman J, Malenka RC, Nicoll RA, Malinow R. Learning mechanisms: the case for CaMKII. *Science* 276: 2001–2002, 1997.

Lisman J, Schulman H, Cline H. The molecular basis of CaMKII function in synaptic and behavioral memory. *Nat Rev Neurosci* 3: 175–190, 2002.

Lisman J, Zhabotinsky AM. A model of synaptic memory: a CaMKII/PP1 switch that potentiates transmission by organizing an AMPA receptor anchoring assembly. *Neuron* 31: 191–201, 2001.

Lledo PM, Hjelmstad GO, Mukherji S, Soderling TR, Malenka RC, Nicoll RA. Calcium/calmodulin-dependent kinase II and long-term potentiation enhance synaptic transmission by the same mechanism. *Proc Natl Acad Sci USA* 92: 11175–11179, 1995.

Malenka RC, Bear MF. LTP and LTD: an embarrassment of riches. *Neuron* 44: 5–21, 2004.

Malenka RC, Nicoll RA. NMDA-receptor-dependent synaptic plasticity: multiple forms and mechanisms. *Trends Neurosci* 16: 521–527, 1993.

Malinow R, Tsien RW. Presynaptic enhancement shown by whole-cell recordings of long-term potentiation in hippocampal slices. *Nature* 346: 177–180, 1990.

Matsushita T, Moriyama S, Fukai T. Switching dynamics and the transient memory storage in a model enzyme network involving Ca^{2+}/calmodulin-dependent protein kinase II in synapse. *Biol Cybern* 72: 497–509, 1995.

Mayer ML, Westbrook GL. Permeation and block of N-methyl-D-aspartic acid receptor channels by divalent cations in mouse cultured central neurones. *J Physiol* 394: 501–527, 1987.

Meyer T, Hanson PI, Stryer L, Schulman H. Calmodulin trapping by calcium-calmodulin-dependent protein kinase. *Science* 256: 1199–1202, 1992.

Michelson S, Schulman H. CaM kinase: a model for its activation and dynamics. *J Theor Biol* 171: 281–290, 1994.

Miller P, Wang XJ. Stability of discrete memory states to stochastic fluctuations in neuronal systems. *Chaos* 16: 26109–26121, 2006.

Miller P, Zhabotinsky AM, Lisman JE, Wang XJ. The stability of a stochastic CaMKII switch: dependence on the number of enzyme molecules and protein turnover. *PLoS Biol* 3: 705–717, 2005.

Miller SG, Kennedy MB. Regulation of brain type II Ca^{2+}/calmodulin-dependent protein kinase by autophosphorylation: a Ca^{2+}-triggered molecular switch. *Cell* 44: 861–870, 1986.

Müller A, Kukley M, Stausberg P, Beck H, Müller W, Dietrich D. Endogenous Ca^{2+} buffer concentration and Ca^{2+} microdomains in hippocampal neurons. *J Neurosci* 25: 558–565, 2005.

Nagerl UV, Novo D, Mody I, Vergara JL. Binding kinetics of calbindin-D_{28k} determined by flash photolysis of caged Ca^{2+}. *Biophys J* 79: 3009–3018, 2000.

Nimchinsky EA, Yasuda R, Oertner TG, Svoboda K. The number of glutamate receptors opened by synaptic stimulation in single hippocampal spines. *J Neurosci* 24: 2054–2064, 2004.

Okamoto H, Ichikawa K. Switching characteristics of a model for biochemical-reaction networks describing autophosphorylation versus dephosphorylation of Ca^{2+}/calmodulin-dependent protein kinase II. *Biol Cybern* 82: 35–47, 2000.

Petersen JD, Chen X, Vinade L, Dosemeci A, Lisman JE, Reese TS. Distribution of postsynaptic density (PSD)-95 and Ca^{2+}/calmodulin-dependent protein kinase II at the PSD. *J Neurosci* 23: 11270–11278, 2003.

Popescu G, Auerbach A. Modal gating of NMDA receptors and the shape of their synaptic response. *Nat Neurosci* 6: 476–483, 2003.

Quintana AR, Wang D, Forbes JE, Waxham MN. Kinetics of calmodulin binding to calcineurin. *Biochem Biophys Res Comm* 334: 674–680, 2005.

Racca C, Stephenson FA, Streit P, Roberts JD, Somogyi P. NMDA receptor content of synapses in stratum radiatum of the hippocampal CA1 area. *J Neurosci* 20: 2512–2522, 2000.

Riveros N, Fiedler J, Lagos N, Munoz C, Orrego F. Glutmate in rat brain cortex synaptic vesicles: influence of the vesicle isolation procedure. *Brain Res* 386: 405–408, 1986.

Rosenmund C, Clements JD, Westbrook GL. Nonuniform probability of glutamate release at a hippocampal synapse. *Science* 262: 754–757, 1993.

Rosenmund C, Feltz A, Westbrook GL. Synaptic NMDA receptor channels have a low open probability. *J Neurosci* 15: 2788–2795, 1995.

Rusakov DA, Kullmann DM. Extrasynaptic glutamate diffusion in the hippocampus: ultrastructural constraints, uptake, and receptor activation. *J Neurosci* 18: 3158–3170, 1998.

Santucci DM, Raghavachari S. The effects of NR2 subunit-dependent NMDA receptor kinetics on synaptic transmission and CaMKII activation. *PLoS Comput Biol* 4: e1000208, 2008.

Schmidt H, Eilers J. Spine neck geometry determines spino-dendritic cross-talk in the presence of mobile endogenous calcium binding proteins. *J Comput Neurosci* 27: 229–243, 2009.

Schmidt H, Kunerth S, Wilms C, Strotmann R, Eilers J. Spino-dendritic cross-talk in rodent Purkinje neurons mediated by endogenous Ca^{2+}-binding proteins. *J Physiol* 581: 619–629, 2007.

Schmidt H, Schwaller B, Eilers J. Calbindin D28k targets *myo*-inositol monophosphatase in spines and dendrites of cerebellar Purkinje neurons. *Proc Natl Acad Sci USA* 102: 5850–5855, 2005.

Shamloo M, Kamme F, Wieloch T. Subcellular distribution and autophosphorylation of calcium/calmodulin-dependent protein kinase II in rat hippocampus in a model of ischemic tolerance. *Neuroscience* 96: 665–674, 2000.

Shifman JM, Choi MH, Mihalas S, Mayo SL, Kennedy MB. Ca^{2+}/calmodulin dependent protein kinase II (CaMKII) is activated by calmodulin with two bound calciums. *Proc Natl Acad Sci USA* 103: 13968–13973, 2006.

Shimozawa T, Murakami J, Kumagai T. Cricket wind receptors: thermal noise for the highest sensitivity known. In: *Sensors and Sensing in Biology and Engineering*, edited by Barth FG, Humphrey JAC, Secomb T. Berlin: Springer-Verlag, 2003, p. 145–157.

Silva AJ, Stevens CF, Tonegawa S, Wang Y. Deficient hippocampal long-term potentiation in alpha-calcium-calmodulin kinase II mutant mice. *Science* 257: 201–206, 1992.

Stemmer PM, Klee CB. Dual calcium ion regulation of calcineurin by calmodulin and calcineurin B. *Biochemistry* 33: 6859–6866, 1994.

Stiles JR, Bartol TM. Monte Carlo methods for simulating realistic synaptic microphysiology using MCell. In: *Computational Neuroscience: Realistic Modeling for Experimentalists,* edited by De Schutter E. Boca Raton, FL: CRC, 2001, p. 87–128.

Takumi Y, Ramirez-Leon V, Laake P, Rinvik E, Ottersen OP. Different modes of expression of AMPA and NMDA receptors in hippocampal synapses. *Nat Neurosci* 2: 618–624, 1999.

Uteshev VV, Pennefather PS. Analytical description of the activation of multi-state receptors by continuous neurotransmitter signals at brain synapses. *Biophys J* 72: 1127–1134, 1997.

Ventriglia F, Maio DV. A Brownian model of glutamate diffusion in excitatory synapses of hippocampus. *Biosystems* 58: 67–74, 2000.

White JA, Rubinstein JT, Kay AR. Channel noise in neurons. *Trends Neurosci* 23: 131–137, 2000.

Xia Z, Storm DR. The role of calmodulin as a signal integrator for synaptic plasticity. *Nat Rev Neurosci* 6: 267–276, 2005.

Yu YG, Wang W, Wang JF, Liu F. Resonance-enhanced signal detection and transduction in the Hodgkin-Huxley neuronal systems. *Phys Rev E* 63: 21907–21918, 2001.

Yuan H, Erreger K, Dravid SM, Traynelis SF. Conserved structural and functional control of *N*-Methyl-D-aspartate receptor gating by transmembrane domain M3. *J Biol Chem* 280: 29708–29716, 2005.

Zeng SY, Jung P. Mechanism for neuronal spike generation by small and large ion channel clusters. *Phys Rev E* 70: 11903–11910, 2004.

Zeng SY, Tang Y, Jung P. Spiking synchronization of ion channel clusters on an axon. *Phys Rev E* 70: 11905–11911, 2007.

Zhabotinsky AM. Bistability in the Ca^{2+}/calmodulin-dependent protein kinase-phosphatase system. *Biophys J* 79: 2211–2221, 2000.

Zhabotinsky AM, Camp RN, Epstein IR, Lisman JE. Role of neurogranin concentrated in spines in the induction of long-term potentiation. *J Neurosci* 26: 7337–7347, 2006.